Aligning 3D Curve with Surface using Tangent and Normal Vectors for Computer-Assisted Orthopedic Surgery

Zhe Min, *Member, IEEE*, Delong Zhu, *Member, IEEE*, Jianbang Liu, *Student Member, IEEE*, Hongliang Ren, *Senior Member, IEEE* and Max Q.-H. Meng*, *Fellow, IEEE*

***Abstract*—Registration that aligns different views of one interested organ together is an essential technique and outstanding problem in medical robotics and image-guided surgery (IGS). This work introduces a novel rigid point set registration (PSR) approach that aims to accurately map the pre-operative space with the intra-operative space to enable successful image guidance for computer-assisted orthopaedic surgery (CAOS). The normal vectors and tangent vectors are first extracted from the pre-operative and intra-operative point sets (PSs) respectively, and are further utilized to enhance the registration accuracy and robustness. The contributions of this article are three-folds. First, we propose and formulate a novel distribution that describes the error between one normal vector and the corresponding tangent vector based on the von-Mises Fisher (vMF) distribution. Second, by modelling the anisotropic position localization error with the multi-variate Gaussian distribution, we formulate the PSR considering anisotropic localization error as a maximum likelihood estimation (MLE) problem and then solve it under the expectation maximization (EM) framework. Third, to facilitate the optimization process, the gradients of the objective function with respect to the desired parameters are computed and presented. Extensive experimental results on the human femur and pelvis models verify that the proposed approach outperforms the state-of-the-art methods, and demonstrate potential clinical values for relevant surgical navigation applications.**

***Index Terms*—Image-to-patient registration, computer-assisted orthopedic surgery (CAOS), anisotropic positional localization error, von-Mises Fisher (vMF) distribution, maximum likelihood estimation (MLE), expectation maximization (EM).**

I. Introduction

WITH 20,0000 annual cases in the USA alone, the anterior cruciate ligament (ACL) rupture is a common medical condition [1]. ACL reconstruction is the procedure where the torn ligament is replaced by a tissue graft, which is pulled into the knee joint through tunnels [1], [2]. Correct tunnel placement (CTP) is crucial for knee ability and maximizing proprioception. However, the performance of CTP depends heavily on the surgeon's operating experience, which varies broadly among different physicians. Some previous studies reveal that only 75% reaches levels of satisfaction with an incidence of revision surgeries being 10% to 15%, half of which is caused by deficient technical execution [3]. In computer-assisted ACL surgery, the pre-operative computed tomography (CT) needs to be registered with the intra-operative points typically collected by an optically tracked surgical pointer. In the total hip replacement (THR) surgery, a failing orthopedic hip implant is replaced with a new one by removing the old implant, by removing the cement and fitting a new implant into an enlarged canal broached in the femur [4]. Computer-assisted surgery for pelvic fracture may cause a high risk of mortality, although the pelvic fractures or surgeries account for 2-8% of all fractures [5].

Generally speaking, computer-assisted surgery (CAS) brings many benefits including stable high accuracy, significantly improved surgical outcomes, and decreased learning curves of novice surgeons [6], [7]. The steps involved in a typical CAS are presented as follows. Before surgery, a computerized surgical plan is tailored for the specific patient in volumetric medical images such as computed tomography (CT) or Magnetic resonance imaging (MRI) [8]. During surgery, the intra-operative data from various modalities such as optically tracked surgical instrument, endoscopic cameras or X-rays in real-time are acquired [9]–[13]. Satisfactory surgical outcome relies on the accurate registration between the pre-defined interventional plan and the intra-operative data in order to achieve the successful interventional image guidance [8], [14]–[16]. Let us consider the rigid point set registration (PSR) problem in the background of computer-assisted orthopedic surgery (CAOS). The pre-operative point set (PS) is acquired by segmenting the interested regions whitin the pre-operative volumetric images while the intra-operative PS is acquired using a optically tracked pointer. Most previous registration methods usually only utilize the positional information contained in the extracted PSs, which are susceptible to noise and outliers. One reason is that finding the correct correspondences between PSs with the presence of noise or outliers is a challenging problem. In this work, in addition to the positional

Zhe Min is with the Department of Medical Physics and Bioengineering, University College London, London, United Kingdom (e-mail: z.min@ucl.ac.uk).

Delong Zhu and Jianbang Liu are with the Department of Electronic Engineering, The Chinese University of Hong Kong, N.T., Hong Kong SAR, China.

Hongliang Ren is with the Department of Electronic Engineering and Shun Hing Institute of Advanced Engineering, The Chinese University of Hong Kong (CUHK), Hong Kong, and also with the Department of Biomedical Engineering, National University of Singapore, Singapore 117575, Singapore (e-mail: hlren@ieee.org).

Max Q.-H. Meng is with the Department of Electronic and Electrical Engineering of the Southern University of Science and Technology in Shenzhen, China, on leave from the Department of Electronic Engineering, The Chinese University of Hong Kong, Hong Kong, and also with the Shenzhen Research Institute of the Chinese University of Hong Kong in Shenzhen, China (e-mail:max.meng@ieee.org).

*Corresponding Anthor.

information, we also utilize the orientational information (i.e., either normal or tangent vectors) extracted from both PSs. Pre-operatively, we extract the normal vectors since that the pre-operative PS is usually dense. Intra-operatively, we extract the tangent vectors from the intra-operative PS. As will be verified in this article, the orientational information extracted from the original raw PSs can help significantly find the correct correspondences.

Related Work PSR problem can be broadly classified into two categories: rigid registration and non-rigid registration [17]–[19]. Rigid registration aims to compute the rigid transformation between two spaces, which includes a rotation matrix, a translation vector and possibly a scaling. Non-rigid registration aims to recover the deformation between two spaces [20]–[23]. Our work focuses on solving the rigid registration problem in an accurate and robust way.

Under the iterative closest point (ICP) framework, the NICP [24] and G-IMOP [25], [26] methods incorporate the estimated surface normal vectors into both correspondence and registration stages of their algorithms. In both orthopedic and cardiac surgeries, both position vectors and normal vectors are utilized to enable intra-operative guidance in both pair-wise [27]–[29] and group-wise generalized PSR problems [30]–[32], and in both rigid [33] and non-rigid PSR problems [27], [28], [30]–[32], [34]. In neurosurgery, the extracted features from the multi-modal brain images could be utilized to screen the outliers [14], [35]. Recent deep-learning based PSR algorithms such as PointNetLK [36], DCP [37] or PRnet [38] first learn high-dimensional features, from which keypoints can then be detected and further used to search the best transformation [36], [39]. Both the above normal-assisted and learning-based registration methods require the PSs to be dense, which may be impractical in many surgical navigation applications. There are also global registration methods such as Fast Global Registration (FGR) method [40], which also requires the PSs to be dense. Under the maximum likelihood (ML) framework, Gaussian Mixture Models- (GMMs-) based probabilistic methods adopt the soft correspondence assignment technique [41]–[43]. Coherent point drift (CPD) [43] method assumes one PS to be generated from the other PS considered as the mixed model's centroids. Expectation conditional maximization for point registration (ECMPR)[42] method generalizes the assumption of isotropic positional error to the anisotropic case. Joint registration of multiple point clouds (JRMPC) method [41] eliminates the bias towards one specific PS in previous methods, by regarding as samples generated from Gaussian Mixture Models whose centres are the rigidly transformed underlying noise-free PS, which was proved to outperform the other advanced methods. Those methods without using extra features, including FGR, CPD, ECMPR and JRMPC, are not robust to noise and outliers.

Motivations and Contributions of Our Work In CAS, the PS segmented from the pre-operative volumetric medical images is dense, from which various features (i.e., normal vectors, lines, planes or fpfh) can be extracted [44]. However, the intra-operative PS usually only forms a curve, from which features such as normal vectors *cannot* be accurately estimated. Hence, most existing feature-based [24], [26], [28], [31], [34], [45] or deep-learning based methods [36]–[38] cannot be readily adopted in the CAOS application. In addition, in many surgical procedures such as the ACL reconstruction, the intra-operative data only covers a partial region of the whole interested organ, and is often corrupted with noise and outliers. With the existing registration methods, finding the correct point correspondences *and* further estimating the correct rigid transformation are still challenging because of the above-mentioned factors including partial overlapping, noise and outliers. To deal with the above challenges, the normal vectors extracted from the pre-operative PS and the tangent vectors estimated from the intra-operative curve are utilized. The anisotropic multi-variate Gaussian distribution is adopted in the proposed method, considering that the position localization error (PLE) in the surgical navigation system is usually anisotropic [46], [47]. Our contributions of this article are both scientific and technical. Scientifically, motivated by the relevant clinical applications, we formulate the problem of registering the pre-operative PS with normal vectors *and* intra-operative PS with tangent vectors as a maximum likelihood estimation (MLE) problem while considering the *anisotropic* localization error. The expectation maximization (EM) technique is used to solve the formulated MLE problem. Technically, to facilitate the computational process, we derive and present gradients of the overall objective function with respect to desired parameters.

Differences from Our Previous Work We have previously proposed several rigid and non-rigid registration methods, which utilize the normal vectors estimated from both PSs to be registered [29], [34], [45], [48], [49]. In those methods, von-Mises Fisher (vMF) distribution was used to model the error distributions between one model normal vector and one data normal vector [29]. The registration problem actually belongs to the category of surface to surface registration, where both PSs have to be dense to accurately estimate the normal vectors. In this paper, we aim to solve the curve to surface registration problem where the pre-operative surface is to be aligned with the intra-operative acquired curve. To enhance the registration performance such as accuracy and robustness, we adopt the tangent vectors estimated from the intra-operative curve and the normal vectors estimated from the pre-operative surface. To model the error distribution between one *model* normal vector and one *data* tangent vector, we modify the original vMF distribution. With the tailored error distribution, the curve to surface rigid registration is formulated as a maximum likelihood estimation (MLE) problem.

This article is organized as follows. Section II presents our proposed curve-to-surface registration method in detail. Section III describes the experiments and associated results. Section IV discusses our proposed approach and future work. Section V concludes this paper. Section VI presents the Appendix that includes derivations of some formulations.

II. Methods

The aim of the rigid point set registration (PSR) problem is to estimate the rotation matrix $\mathbf{R} \in SO(3)$ and the translation vector $\mathbf{t} \in \mathbb{R}^3$ given two point sets (PSs)

$\{\mathbf{y}_m\}_{m=1}^{M}(M \in \mathbb{N}^+)$ and $\{\mathbf{x}_n\}_{n=1}^{N}$ $(N \in \mathbb{N}^+)$. Let us denote $\mathbf{X} = [\mathbf{x}_1, ..., \mathbf{x}_n, ..., \mathbf{x}_N] \in \mathbb{R}^{3\times N}(M \in \mathbb{N}^+)$ and $\mathbf{Y} = [\mathbf{y}_1, ..., \mathbf{y}_m, ..., \mathbf{y}_M] \in \mathbb{R}^{3\times M}(N \in \mathbb{N}^+)$. In our proposed algorithm, the tangent vectors $\widehat{\mathbf{X}} = [\widehat{\mathbf{x}}_1, ..., \widehat{\mathbf{x}}_N] \in \mathbb{R}^{3\times N}$ and normal vectors $\widehat{\mathbf{Y}} = [\widehat{\mathbf{y}}_1, ..., \widehat{\mathbf{y}}_M] \in \mathbb{R}^{3\times M}$ are also utilized, which can be extracted from $\mathbf{X}$ and $\mathbf{Y}$. In image-guided surgery (IGS), the model PS $\mathbf{Y}$ is the PS segmented from the pre-operative volumetric medical images while the data PS $\mathbf{X}$ denotes the intra-operative PS. We formulate the PSR problem as a maximum likelihood estimate (MLE) one, and solve the problem with the expectation maximization technique. The overall registration scheme is the following: (a) construct the probabilistic models associated with the positional vectors $\mathbf{X}$ and orientational vectors $\widehat{\mathbf{X}}$; (b) formulate the MLE problem that is to be solved with respect to the desired parameters including $\mathbf{R}$ and $\mathbf{t}$; (c) derive the formulas of the iterative expectation maximization (EM) steps in solving the MLE problem.

A. Illustration of the modified vMF distribution

There is no off-the-shelf probability distribution to quantify the error between a sample tangent vector and the central normal vector of that distribution from which the tangent vector is generated. In order to model the error distribution between a normal vector and the corresponding tangent vector, we correspondingly modify the original von-Mises Fisher (vMF) distribution that describes the error between two normal vectors to a new distribution. The probability density function (PDF) of the modified vMF distribution

$$p(\widehat{\mathbf{x}}_n|\mathbf{R}\widehat{\mathbf{y}}_m) = \frac{\kappa}{2\pi(e^{\kappa} - e^{-\kappa})} e^{\kappa||\mathbf{R}\widehat{\mathbf{y}}_m \times \widehat{\mathbf{x}}_n||} \tag{1}$$

gives the probability of $\widehat{\mathbf{x}}_n$ being generated by $\mathbf{R}\widehat{\mathbf{y}}_m$, where $\kappa \in \mathbb{R}$ is the concentration parameter, $\times$ denotes the cross product of two vectors. In the context of our paper, $\widehat{\mathbf{y}}_m$ represent the pre-operative normal vectors while $\widehat{\mathbf{x}}_n$ represent the intra-operative tangent vectors. The above distribution $p(\widehat{\mathbf{x}}_n|\mathbf{R}\widehat{\mathbf{y}}_m)$ gives the probability that one data tangent vector $\widehat{\mathbf{x}}_n$ is sampled from the corresponding transformed model normal vector $\mathbf{R}\widehat{\mathbf{y}}_m$. Let $\widehat{\mathbf{x}}_n^{\perp} \in \mathbb{R}^3$ ($||\widehat{\mathbf{x}}_n^{\perp}|| = 1$) denote the normal vector that is orthogonal to $\widehat{\mathbf{x}}_n$ at the point $\mathbf{x}_n$(i.e. $\widehat{\mathbf{x}}_n^{\mathsf{T}}\widehat{\mathbf{x}}_n^{\perp} = 0$, and $||\widehat{\mathbf{x}}_n^{\perp}|| = 1$). In all the following cases, $\widehat{\mathbf{x}}_n$ and $\widehat{\mathbf{x}}_n^{\perp}$ lie in one common plane $\mathcal{P}$ *while* $\widehat{\mathbf{x}}_n^{\perp}$ and the rotated model normal vector $\mathbf{R}\widehat{\mathbf{y}}_m$ lie in the other plane $\mathcal{Q}$. As it is shown in Fig. 1, let $\theta_1 \in \mathbb{R}$ denote the angle between $\mathbf{R}\widehat{\mathbf{y}}_m$ and the tangent vector $\widehat{\mathbf{x}}_n$ while $\theta_2 \in \mathbb{R}$ denote the angle between $\mathbf{R}\widehat{\mathbf{y}}_m$ and $\widehat{\mathbf{x}}_n^{\perp}$. In Case One, the three vectors (i.e., $\widehat{x}_n$, $\mathbf{R}\widehat{\mathbf{y}}_m$, and $\widehat{\mathbf{x}}_n^{\perp}$) lie in one common plane $\mathcal{P}$, and $\theta_1 < \frac{\pi}{2}$, $\theta_2 < \frac{\pi}{2}$. As shown in Fig. 1 (Case One), $\theta_2 = \frac{\pi}{2} - \theta_1$ holds, resulting $\cos(\theta_2) = \cos(\frac{\pi}{2} - \theta_1) = \sin(\theta_1)$. Thus, the cross product $\mathbf{R}\widehat{\mathbf{y}}_m \times \widehat{\mathbf{x}}_n$ (i.e., $\sin(\theta_1)$) is utilized in our case to replace the dot product $(\mathbf{R}\widehat{\mathbf{y}}_m)^{\mathsf{T}}\widehat{\mathbf{x}}_n^{\perp}$. In Case Two, the three vectors lie in common plane $\mathcal{P}$, $\theta_2 < \frac{\pi}{2}$ while $\theta_1 > \frac{\pi}{2}$. As shown in Fig. 1 (Case Two), $\theta_1 = \frac{\pi}{2} + \theta_2$ holds, resulting the equation $\cos(\theta_2) = \cos(\theta_1 - \frac{\pi}{2}) = \cos(\frac{\pi}{2} - \theta_1) = \sin(\theta_1)$. In Case Three, as shown in Fig. 1 (Case Three), $\widehat{\mathbf{x}}_n \in \mathcal{P}$ and $\widehat{\mathbf{x}}_n^{\perp} \in \mathcal{P}$ while $\mathbf{R}\widehat{\mathbf{y}}_m$ lies in a different plane. In this case, we notice that if θ_1(in the range [0,90]°) becomes larger, θ_2(in the range [0,90]°) will become smaller accordingly. Thus, it is appropriate to use $\sin(\theta_1)$ to replace $\cos(\theta_2)$. In the last extreme case (i.e., Case Four), as shown in Fig. 1 (Case Four), $\theta_1 = \frac{\pi}{2}$ regardless of the values of θ_2. By summarizing the above four cases, we can see that the dot product of two normal vectors is equal to the cross product of a tangent vector and a normal vector.

B. Rigid Point Set Registration with Normal and Tangent Vectors

Now we have the PDF that describes the error between one normal vector and its corresponding tangent vector, we are able to cast the registration into an optimization problem. With the latent variables being the point correspondences in two PSs, the registration of two generalized PSs is formulated as a MLE problem. The MLE problem is readily solved under the expectation maximization (EM) framework. More specifically, in the expectation step, the point correspondences are computed given the other parameters (either from the initialization at the beginning of the algorithm or from last EM step). In the maximization step, the rotation matrix, translation vector, positional covariance matrix and the concentration parameter are updated given the other parameters. In what follows, we first construct the objective function to be minimized. Afterwards, the detailed EM steps are derived and presented.

The Hybrid Mixture Models Since we are registering generalized points that include positional vectors and normal (or tangent) vectors in two spaces, the probability density function has to be defined. To proceed, the positional vectors and orientational vectors are assumed to be independent in both spaces to be registered [31]. The multi-variate Gaussian distribution is utilized to model the localization error associated with the positional vectors. With the above (modified vMF) distribution presented in (1), the probability of one generalized intra-operative data point $\mathbf{d}_n^x = [\mathbf{x}_n^{\mathsf{T}}, \widehat{\mathbf{x}}_n^{\mathsf{T}}]^{\mathsf{T}} \in \mathbb{R}^6$ being generated by the transformed model point $\mathbf{d}_m^y = [(\mathbf{R}\mathbf{y}_m + \mathbf{t})^{\mathsf{T}}, (\mathbf{R}\widehat{\mathbf{y}}_m)^{\mathsf{T}}]^{\mathsf{T}}$ given the correspondence $z_n = m$ and model parameters $\mathbf{\Theta}$ (which will be defined below) is the product of the anisotropic multi-variate Gaussian distribution and the modified vMF distribution as follows

$$\begin{aligned} &p(\mathbf{d}_n^x|z_n = m, \mathbf{\Theta}) \\ &= \underbrace{\frac{1}{(2\pi)^{\frac{3}{2}}|\mathbf{\Sigma}|^{\frac{1}{2}}} e^{\frac{-1}{2}\left(\mathbf{x}_n - (\mathbf{R}\mathbf{y}_m + \mathbf{t})\right)^{\mathsf{T}}\mathbf{\Sigma}^{-1}\left(\mathbf{x}_n - (\mathbf{R}\mathbf{y}_m + \mathbf{t})\right)}}_{\text{Anisotropic Multivariate Gaussian Distribution}} \\ &\underbrace{\frac{\kappa}{2\pi(e^{\kappa} - e^{-\kappa})} e^{\kappa||\mathbf{R}\widehat{\mathbf{y}}_m \times \widehat{\mathbf{x}}_n||}}_{\text{Modified vMF Distribution}}, \end{aligned} \tag{2}$$

where $\mathbf{d}_n^x = [\mathbf{x}_n^{\mathsf{T}}, \widehat{\mathbf{x}}_n^{\mathsf{T}}]^{\mathsf{T}} \in \mathbb{R}^6$, $\mathbf{\Sigma} \in \mathcal{S}^3$ is the symmetric positional covariance matrix, $|\mathbf{\Sigma}|$ denotes the determinant of $\mathbf{\Sigma}$, $\kappa \in \mathbb{R}$ is the concentration parameter associated with the orientational error, $z_n \in \mathbb{N}^+$ is the correspondence variable ($z_n = m$ if $\widehat{\mathbf{x}}_n$ corresponds to $\widehat{\mathbf{y}}_m$), the model parameter set is $\mathbf{\Theta} = \{\mathbf{R}, \mathbf{t}, \kappa, \mathbf{\Sigma}\}$. The inherent rationale, with $z_n = m$, is that the data positional vector $\mathbf{x}_n$ and the data tangent vector $\widehat{\mathbf{x}}_n$ are respectively randomly sampled from the multi-variate Gaussian distribution (with the covariance matrix $\mathbf{\Sigma}$) centered

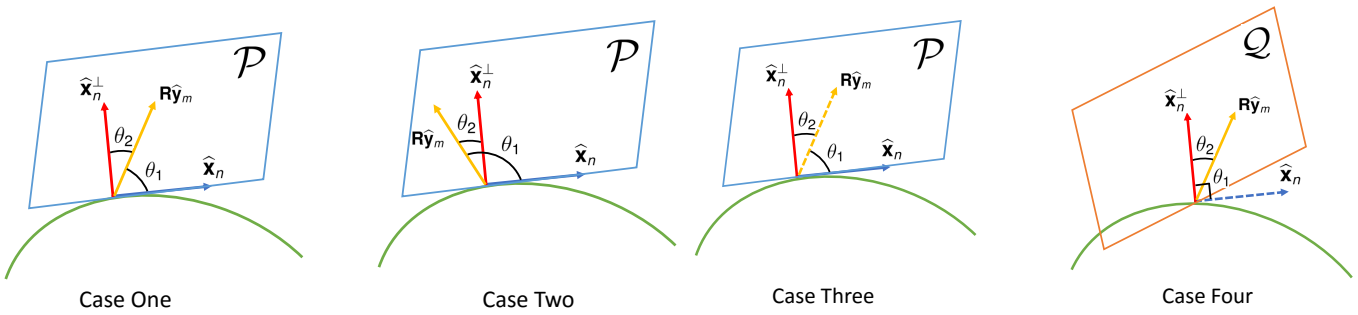

Fig. 1. Illustration of the novel modified vMF distribution, case one to case four. In Case One and Two, all three vectors $\mathbf{R}\widehat{\mathbf{y}}_m$ (the rotated model normal vector), $\widehat{\mathbf{x}}_n^{\perp}$ (the data normal vector) and $\widehat{\mathbf{x}}_n$ (the data tangent vector) lie in the same plane $\mathcal{P}$. In Case Three, $\widehat{\mathbf{x}}_n^{\perp}$ and $\widehat{\mathbf{x}}_n$ lie in the common plane $\mathcal{P}$ while the transformed model normal vector $\mathbf{R}\widehat{\mathbf{y}}_m$ lie in another plane. In Case Four, $\mathbf{R}\widehat{\mathbf{y}}_m$ and $\widehat{\mathbf{x}}_n^{\perp}$ lie in the common plane $\mathcal{Q}$ while $\widehat{\mathbf{x}}_n$ lies in another plane.

at the transformed model position vector $\mathbf{R}\mathbf{y}_m + \mathbf{t}$ *and* the modified vMF distribution (with the concentration parameter κ) centered at the transformed model normal vector $\mathbf{R}\widehat{\mathbf{y}}_m$.

To seek the optimal model parameters $\boldsymbol{\Theta}$, by assuming the independence of all the data points (which is a common and needed assumption in PSR algorithms), the likelihood defined as $\boldsymbol{\Theta} = \arg\max_{\boldsymbol{\Theta}} p(\mathbf{D}_x|\mathbf{D}_y, \boldsymbol{\Theta}) = \prod_{n=1}^{N} p(\mathbf{d}_n^x|z_n = m, \boldsymbol{\Theta})$ (where $\mathbf{D}_x$ includes all the $\mathbf{d}_n^x$ and $\mathbf{T}(\mathbf{D_y})$ includes all the $\mathbf{T}(\mathbf{d_m^y}) = [(\mathbf{R}\mathbf{y}_m + \mathbf{t})^{\mathsf{T}}, (\mathbf{R}\widehat{\mathbf{y}}_m)^{\mathsf{T}}]^{\mathsf{T}} \in \mathbb{R}^6$) needs to be maximized with respect to $\boldsymbol{\Theta}$. However, in practice, the negative log likelihood $-\log p(\mathbf{D}_x|\mathbf{T}(\mathbf{D_y}), \boldsymbol{\Theta})$ is usually minimized to estimate $\boldsymbol{\Theta}$ as follows

$$\begin{aligned}\boldsymbol{\Theta} &= -\arg\min_{\Theta} \log p(\mathbf{D}_x|\mathbf{D}_y, \boldsymbol{\Theta}) \\ &= -\arg\min_{\Theta} \log \prod_{n=1}^{N} p(\mathbf{d}_n^x|\mathbf{D}_y, \boldsymbol{\Theta}) \\ &= \arg\max_{\Theta} \sum_{n=1}^{N} \log p(\mathbf{d}_n^x|\mathbf{D}_y, \boldsymbol{\Theta})\end{aligned} \tag{3}$$

where the expression of the hybrid mixture model (HMM) $p(\mathbf{d}_n^x|\mathbf{D}_y, \boldsymbol{\Theta})$ is

$$p(\mathbf{d}_n^x|\mathbf{D}_y, \boldsymbol{\Theta}) = (1-w)\sum_{m=1}^{M}\frac{1}{M}p(\mathbf{d}_n^x|z_n = m, \boldsymbol{\Theta}) + w\frac{1}{N} \tag{4}$$

which is the sum of an additional uniform distribution (to account for noise or outliers) *and* the PDF in (2), $w \in \mathbb{R}$ is the weighting factor of the outlier distribution in the HMMs and the expression of $p(\mathbf{d}_n^x|z_n = m, \boldsymbol{\Theta})$ is defined in (2).

The Objective Function Similar to the derivations in [29], by (i) substituting (2) into (4) and by substituting the updated (4) into (3); (ii) retaining the terms that are related with the rotation matrix $\boldsymbol{\Theta}$, the overall objective function $Q(\boldsymbol{\Theta})$ to be minimized is defined as follows,

$$\begin{aligned}&\sum_{n=1}^{N}\sum_{m=1}^{M} p_{mn}\left(\frac{1}{2}\big(\mathbf{x}_n - (\mathbf{R}\mathbf{y}_m + \mathbf{t})\big)^{\mathsf{T}}\boldsymbol{\Sigma}^{-1}\big(\mathbf{x}_n - (\mathbf{R}\mathbf{y}_m + \mathbf{t})\big)\right. \\ &\left. - \kappa||(\mathbf{R}\widehat{\mathbf{y}}_m) \times \widehat{\mathbf{x}}_n||\right) + \frac{1}{2}N_{\mathbf{P}}\log|\boldsymbol{\Sigma}| + N_{\mathbf{P}}\log(e^{\kappa} - e^{-\kappa}) \\ &- N_{\mathbf{P}}\log\kappa\end{aligned} \tag{5}$$

where the sum of the posteriors is $N_{\mathbf{P}} = \sum_{n=1}^{N}\sum_{m=1}^{M} p_{mn}$. When the objective function $Q(\boldsymbol{\Theta})$ is minimized, two nonlinear constraints have to be satisfied: (1) $\mathbf{R}\mathbf{R}^{\mathsf{T}} = 1$; (2) $\det(\mathbf{R}) = +1$. Iterative EM technique is adopted to solve the above optimization problem with the missing data being the point correspondence probabilities p_{mn}. At the beginning of the algorithm, the rotation matrix $\mathbf{R}^0$ and translation vector $\mathbf{t}^0$ are initialized to be the 3-by-3 identity matrix and 3-by-1 zero vector respectively.

Expectation Step In this step, we compute the correspondence probabilities p_{mn} given the rotation matrix $\mathbf{R}$, the translation vector $\mathbf{t}$, the positional covariance matrix $\boldsymbol{\Sigma}$ and the concentration parameter κ in the last iterative step. Posterior probabilities $\{p_{mn}\}_{n,m=N,M} \in \mathbb{R}$ are updated based on the Bayes' rule as

$$p_{mn} = \frac{P(m)|p(\mathbf{d}_n|z_n = m, \boldsymbol{\Theta})}{p(\mathbf{d}_n^x|\mathbf{D}_y, \boldsymbol{\Theta})} \tag{6}$$

where the expression of is $p(\mathbf{d}_n^x|\mathbf{D}_y, \boldsymbol{\Theta})$ is in (4). The posterior is stored in the new matrix $\mathbf{P}(m, n) = p_{mn}$, where p_{mn} means the probability that m-th model point $(\mathbf{R}\mathbf{y}_m + \mathbf{t}, \mathbf{R}\widehat{\mathbf{y}}_m)$ corresponds to the n-th data point $\mathbf{d}_n^x$.

Maximization Transformation Step In this step, the rotation matrix $\mathbf{R}$ and translation vector $\mathbf{t}$ are updated given the other parameters. Instead of seeking the parameters $\mathbf{R}$ and $\mathbf{t}$ directly, the incremental rotation matrix $d\mathbf{R} \in SO(3)$ and $d\mathbf{t} \in \mathbb{R}^3$ between two iterative Maximization Transformation steps (e.g., q and q+1 steps) are estimated. After manipulating the corresponding derivations, the objective function $Q(d\mathbf{R}, d\mathbf{t})$ related with $(d\mathbf{R}, d\mathbf{t})$ to be *minimized* is as follows

$$\begin{aligned}Q(d\mathbf{R}, d\mathbf{t}) = \sum_{n,m=1}^{N,M}\Bigg(&\underbrace{\frac{1}{2}p_{mn}^q\mathbf{z}_{mn}^{\mathsf{T}}\boldsymbol{\Sigma}^{-1}\mathbf{z}_{mn} - \frac{1}{2}p_{mn}^q\mathbf{x}_n^{\mathsf{T}}\boldsymbol{\Sigma}^{-1}\mathbf{x}_n}_{\text{Positional Part } C_{P,mn}\in\mathbb{R}} \\ &\underbrace{-p_{mn}^q\kappa\Big|\Big|(d\mathbf{R}\mathbf{R}^{q-1}\widehat{\mathbf{y}}_m) \times \widehat{\mathbf{x}}_n\Big|\Big|}_{\text{Orientational Part } C_{N,mn}\in\mathbb{R}}\Bigg),\end{aligned} \tag{7}$$

where $q \in \mathbb{N}^+$ represent the index of the current iteration, $\mathbf{z}_{mn} = \mathbf{x}_n - d\mathbf{R}(\mathbf{R}^{q-1}\mathbf{y}_m + \mathbf{t}^{q-1}) - d\mathbf{t}$, $p_{mn}^q \in \mathbb{R}$ is the posterior probability in the current step. Considering that $d\mathbf{R}$ and $d\mathbf{t}$ together denote the transformation matrix between two iterative steps, the m-th central point at the

current step $\mathbf{R}\mathbf{y}_m + \mathbf{t}$ is the transformed central point at the last iteration $\mathbf{R}^{q-1}\mathbf{y}_m + \mathbf{t}^{q-1}$ using $d\mathbf{R}$ and $d\mathbf{t}$, i.e. $d\mathbf{R}(\mathbf{R}^{q-1}\mathbf{y}_m + \mathbf{t}^{q-1}) - d\mathbf{t}$. The derivation of (7) from (5) is simple, using $\mathbf{z}_{mn}$ to replace $(\mathbf{x}_n - (\mathbf{R}\mathbf{y}_m + \mathbf{t})$ in (5). The term $-\frac{1}{2}p_{mn}^q \mathbf{x}_n^\mathsf{T}\mathbf{\Sigma}^{-1}\mathbf{x}_n$ appears in (7) is because this term is irrelevant with either $d\mathbf{R}$ or $d\mathbf{t}$ while the subtracted terms are either related with $d\mathbf{R}$ or $d\mathbf{t}$. The readers should note that the overall objective function $Q(d\mathbf{R}, d\mathbf{t})$ consists of two parts: $C_{P,mn}$ that is related with the positional vectors $\{\mathrm{X},\mathrm{Y}\}$ and $C_{N,mn}$ that is related with the orientational vectors $\{\widehat{\mathbf{X}}, \widehat{\mathbf{Y}}\}$. In addition, the incremental rotation matrix $d\mathbf{R}$ is represented using the Rodrigues rotation formula,

$$\mathbf{R}(\boldsymbol{\theta}) = \mathbf{I} + \frac{\sin(\vartheta)}{\vartheta}[\boldsymbol{\theta}]_\times + \frac{1-\cos(\vartheta)}{\vartheta^2}[\boldsymbol{\theta}]_\times^2, \tag{8}$$

where $[\boldsymbol{\theta}]_\times$ denotes the asymmetrical matrix constructed from $\boldsymbol{\theta} \in \mathbb{R}^3$.Specifically, $d\mathbf{R} = \mathbf{R}(d\boldsymbol{\theta})$, where $d\boldsymbol{\theta} \in \mathbb{R}^3$ denotes the incremental rotation angle, with which $Q(d\mathbf{R}, d\mathbf{t})$ is converted into $Q(d\boldsymbol{\theta}, d\mathbf{t})$. To optimize one objective function, the gradient descent method is usually adopted where the gradients can be either in analytical forms or computed numerically. Here we present the gradients for improving the computational speed.

Gradients In order to speed up the computation process, we compute and provide the gradients of $Q(d\boldsymbol{\theta}, d\mathbf{t})$ with respect to $d\boldsymbol{\theta}$ and $d\mathbf{t}$. The computation of the gradients can be divided into five steps. *First*, we rewrite the orientational part $C_{N,mn}$ in (7) as

$$C_{N,mn} = -p_{mn}^q \kappa \sqrt{1 - (\widehat{\mathbf{y}}_m^\mathsf{T}\mathbf{R}^\mathsf{T} d\mathbf{R}^\mathsf{T}\widehat{\mathbf{x}}_n)^2}, \tag{9}$$

The detailed derivation of (9) is presented in Section. VI-B. With (9), we can compute the gradient of the orientational part with respect to $d\mathbf{R}$ $\frac{\partial \mathbf{C}_{N,mn}}{\partial d\mathbf{R}}$ as

$$p_{mn}^q \kappa \widehat{\mathbf{y}}_m^\mathsf{T}\mathbf{R}^\mathsf{T} d\mathbf{R}^\mathsf{T}\widehat{\mathbf{x}}_n \Big(1 - (\widehat{\mathbf{y}}_m^\mathsf{T}\mathbf{R}^\mathsf{T} d\mathbf{R}^\mathsf{T}\widehat{\mathbf{x}}_n)^2\Big)^{-\frac{1}{2}} \widehat{\mathbf{x}}_n \widehat{\mathbf{y}}_m^\mathsf{T}\mathbf{R}^\mathsf{T}, \tag{10}$$

whose detailed derivation is given in Section. VI-C. By substituting (10) into the following (i.e., the gradient of $\partial \mathbf{C}_{N,mn}$ with respect to $d\theta_i$)

$$\frac{\partial \mathbf{C}_{N,mn}}{\partial d\theta_i} = \mathrm{trace}\Big[(\frac{\partial \mathbf{C}_{N,mn}}{\partial d\mathbf{R}})^\mathsf{T}\frac{\partial d\mathbf{R}}{d\theta_i}\Big], i = 1,2,3, \tag{11}$$

we can compute $\frac{\partial \mathbf{C}_{N,mn}}{\partial d\theta_i}(i = 1,2,3)$. The readers should note that $\frac{\partial \mathbf{C}_{N,mn}}{\partial dt_i} = 0(i = 1,2,3)$ since that $\mathbf{C}_{N,mn}$ is related with the normal vectors and tangent vectors. The derivations and expressions of $\frac{\partial \mathbf{C}_{P,mn}}{\partial d\theta_i}(i = 1,2,3)$, $\frac{\partial \mathbf{C}_{P,mn}}{\partial dt_i}(i = 1,2,3)$ and $\frac{\partial d\mathbf{R}}{d\theta_i}(i = 1,2,3)$ are similar with those in [45]. For the convenience of readers, we include the expressions of $\frac{\partial d\mathbf{R}}{d\theta_i}(i = 1,2,3)$ and $\frac{\partial \mathbf{C}_{P,mn}}{\partial d\mathbf{t}}(i = 1,2,3)$ in Section VI-D and Section VI-E, respectively. *Third*, the Jacobians of $C_{P,mn}$ with respect to $\mathrm{d}\theta$ and $\mathrm{d}\mathbf{t}$, and the Jacobians of $C_{N,mn}$ with respect to $\mathrm{d}\theta$(for $n = 1:N$ *and* $m = 1:M$) are respectively

$$\begin{cases} \mathbf{J}_{C_{P,mn},d\boldsymbol{\theta}} = [\frac{\partial \mathbf{C}_{P,mn}}{\partial d\theta_1}, \frac{\partial \mathbf{C}_{P,mn}}{\partial d\theta_2}, \frac{\partial \mathbf{C}_{P,mn}}{\partial d\theta_3}] \in \mathbb{R}^{1\times 3} \\ \mathbf{J}_{C_{P,mn},d\mathbf{t}} = [\frac{\partial \mathbf{C}_{P,mn}}{\partial dt_1}, \frac{\partial \mathbf{C}_{P,mn}}{\partial dt_2}, \frac{\partial \mathbf{C}_{P,mn}}{\partial dt_3}] \in \mathbb{R}^{1\times 3} \\ \mathbf{J}_{C_{N,mn},d\boldsymbol{\theta}} = [\frac{\partial \mathbf{C}_{N,mn}}{\partial d\theta_1}, \frac{\partial \mathbf{C}_{N,mn}}{\partial d\theta_2}, \frac{\partial \mathbf{C}_{N,mn}}{\partial d\theta_3}] \in \mathbb{R}^{1\times 3} \end{cases}, \tag{12}$$

which can be easily constructed. *Fourth*, the overall gradients are the transpose of the concatenated Jacobian vectors,

$$\begin{cases} \bigtriangledown \mathbf{C}_{P,mn} = [\mathbf{J}_{C_{P,mn},d\boldsymbol{\theta}}, \mathbf{J}_{C_{P,mn},d\mathbf{t}}]^\mathsf{T} \in \mathbb{R}^{6\times 1} \\ \bigtriangledown \mathbf{C}_{N,mn} = [\mathbf{J}_{C_{N,mn},d\boldsymbol{\theta}}, \mathbf{0}_{1\times 3}]^\mathsf{T} \in \mathbb{R}^{6\times 1} \end{cases}, \tag{13}$$

Finally, the sum of gradients of the objective function $\mathbf{C}$ with respect to the desired parameters $d\theta, d\mathbf{t}$ are

$$\bigtriangledown \mathbf{C} = \sum_{n=1}^{N}\sum_{m=1}^{M} \bigtriangledown \mathbf{C}_{P,mn} + \sum_{n=1}^{N}\sum_{m=1}^{M} \bigtriangledown \mathbf{C}_{N,mn}, \tag{14}$$

With the gradients, we utilize the *trust-region method* to solve the optimization problem in (7). After getting the $d\theta$ and $d\mathbf{t}$, we can use (8) to get the incremental rotation $\mathrm{d}\mathbf{R}$ and $d\mathbf{t}$. The updated rotation matrix and translation vector are updated as $\mathbf{R}^q = d\mathbf{R}\mathbf{R}^{q-1}$ and $\mathbf{t}^q = d\mathbf{R}\mathbf{t}^{q-1} + d\mathbf{t}$ in the current step, where $\mathbf{R}^{q-1}$ and $\mathbf{t}^{q-1}$ denote the updated rotation matrix and transaltion vector in the last step.

Maximization Covariance Step In this step, the positional covariance matrix $\mathbf{\Sigma}$ is updated given other parameters. The terms of $Q(d\mathbf{R}, d\mathbf{t})$ in (7) that are related with $\mathbf{\Sigma}$, i.e. $Q(\mathbf{\Sigma})$ are as follows,

$$Q(\mathbf{\Sigma}) = \sum_{n,m=1}^{N,M} \left(\frac{1}{2}p_{mn}^q \mathbf{z}_{mn}^\mathsf{T}\mathbf{\Sigma}^{-1}\mathbf{z}_{mn} - \frac{1}{2}p_{mn}^q \mathbf{x}_n^\mathsf{T}\mathbf{\Sigma}^{-1}\mathbf{x}_n\right). \tag{15}$$

The positional covariance matrix $\mathbf{\Sigma}^q$ is updated by solving $\frac{\partial Q(\mathbf{\Theta})}{\partial \mathbf{\Theta}} = \mathbf{0}$:

$$\begin{aligned} \mathbf{\Sigma}^q = \Big(&\mathbf{X}\mathrm{diag}\big(\mathbf{P}^\mathsf{T}\mathbf{1}\big)\mathbf{X}^\mathsf{T} - \mathbf{X}\mathbf{P}^\mathsf{T}\mathbf{1}\mathbf{t}^\mathsf{T} - \mathbf{t}\mathbf{1}^\mathsf{T}\mathbf{P}\mathbf{X}^\mathsf{T} + \mathbf{R}\mathbf{Y}\mathbf{P}\mathbf{1}\mathbf{t}^\mathsf{T} \\ &+ \mathbf{t}\mathbf{1}^\mathsf{T}\mathbf{P}^\mathsf{T}\mathbf{Y}^\mathsf{T}\mathbf{R}^\mathsf{T} - \mathbf{R}\mathbf{Y}\mathbf{P}\mathbf{X}^\mathsf{T} - \mathbf{X}\mathbf{P}^\mathsf{T}\mathbf{Y}^\mathsf{T}\mathbf{R}^\mathsf{T} + \mathbf{t}\mathbf{t}^\mathsf{T}N_\mathbf{P} \\ &+ \mathbf{R}\mathbf{Y}\mathrm{diag}(\mathbf{P}\mathbf{1})\mathbf{Y}\mathbf{P}^\mathsf{T}\mathbf{R}^\mathsf{T}\Big)/N_\mathbf{P}, \end{aligned} \tag{16}$$

where $\mathbf{1}$ is a column vector of all elements being 1 with the appropriate dimension. For example, the $\mathbf{1}$ in $\mathbf{P}^\mathsf{T}\mathbf{1}$ is $\mathbb{R}^{M\times 1}$ since $\mathbf{P}$ is $\mathbb{R}^{M\times N}$. As another example, the $\mathbf{1}$ in $\mathbf{t}\mathbf{1}^\mathsf{T}\mathbf{P}^\mathsf{T}\mathbf{Y}^\mathsf{T}\mathbf{R}^\mathsf{T}$ is $\mathbb{R}^{N\times 1}$ in order to the matrix (or vector mulplication) since $\mathbf{P}$ is $\mathbb{R}^{M\times 1}$.

Maximization κ step In this step, the concentration parameter κ associated with the orientational vectors $\widehat{\mathbf{X}}$ is updated given other parameters. By retaining the terms that are related with κ, the objective function $Q(d\mathbf{R}, d\mathbf{t})$ in (7) becomes

$$\begin{aligned} Q(\kappa) = &-\kappa\sum_{n=1}^{N}\sum_{m=1}^{M} p_{mn}||\mathbf{R}\widehat{\mathbf{y}}_m \times \widehat{\mathbf{x}}_n|| + N_\mathbf{P}\log(e^\kappa - e^{-\kappa}) \\ &- N_\mathbf{P}\log(\kappa) \end{aligned}. \tag{17}$$

The concentration parameter κ is updated by solving the equation $\frac{\partial Q(\kappa)}{\partial \kappa} = 0$, i.e.,

$$-\frac{1}{\kappa} + \frac{e^\kappa + e^{-\kappa}}{e^\kappa - e^{-\kappa}} = \frac{1}{N_\mathbf{P}}\sum_{m=1}^{M}\sum_{n=1}^{N} p_{mn}||\mathbf{R}\widehat{\mathbf{y}}_m \times \widehat{\mathbf{x}}_n||. \tag{18}$$

The closed-form solution to updating κ, as those in [26], [29], as

$$\kappa = r(3 - r^2)/(1 - r^2), \tag{19}$$

where $r = r_1 + r_2$ with r_1 and r_2 being the following

$$\begin{cases} r_1 = \frac{1}{N_{\mathbf{P}}} \sum_{n=1}^{N} \sum_{m=1}^{M} p_{mn} ||\mathbf{R}\widehat{\mathbf{y}}_m \times \widehat{\mathbf{x}}_n|| \\ r_2 = \frac{\sum_{n=1}^{N} \sum_{m=1}^{M} p_{mn} \mathbf{x}_n'^{\mathsf{T}} \mathbf{R} \mathbf{y}_m'}{p_{mn} ||\mathbf{R}\mathbf{y}_m'|| ||\mathbf{x}_n'||} \end{cases}, \tag{20}$$

where $\mathbf{x}_n'$ and $\mathbf{y}_m'$ are the demeaned positional vectors as those in [29]. The above expectation and maximization procedures are iterated until convergence to acquire the final registration result $[\mathbf{R}, \mathbf{t}]$.

III. Experiments and Results

A. Results on the Human Pelvis and Femur Data

In this experiment, we first validate the proposed approach on the data generated from human femur models in the clinical background of total hip replacement (THR) surgery [52]. In the total hip replacement procedure, the femur bone model is used and the intra-operative points cover a partial region of the whole pre-operative model (i.e. the femur head). The intra-operative points can be acquired by optically tracked surgical pointer or laser range scanner (LRS). The experiments on the femur model are 'partial' to 'full' registrations. We also perform experiments on the human pelvis model, where the intra-operative PSs are uniformly sampled from the whole pre-operative model. The experiments on the human pelvis model are 'full' to 'full' registrations. The pre-operative PS is assumed as the model PS $\mathbf{Y}$(where $M = 1568$ points exist) while the intra-operative PS is considered as the data PS $\mathbf{X}$ (where $N_{\text{trial}} = 100$ inlier points exist). The normal vectors $\widehat{\mathbf{Y}}$ are computed using the *principal component analysis* (PCA) technique [29]. To test the proposed approach's robustness to noise and outliers, noise and outliers are injected into $\mathbf{X}$ and $\widehat{\mathbf{X}}$. On one hand, randomly generated isotropic and anisotropic positional noise vectors are injected into $\mathbf{X}$: $\mathbf{\Sigma}_{\text{iso}} = \text{diag}([\frac{1}{3}, \frac{1}{3}, \frac{1}{3}])$ *and* $\mathbf{\Sigma}_{\text{aniso}} = \text{diag}([\frac{1}{11}, \frac{1}{11}, \frac{9}{11}])$ [1]. On the other hand, the tangent vectors $\widehat{\mathbf{X}}$ are corrupted with randomly generated isotropic orientational error at 1° standard deviation (i.e. $\kappa = 3200$). Five different percentages of outliers are injected into $\mathbf{X}$ and $\widehat{\mathbf{X}}$: $10\%, 30\%, 50\%, 70\%, 90\%$. As an example, the number of all intra-operative points is $N_{\text{all}} = N \times (1 + 10\%)$ when there exists 10% outliers. The rotational angle and the translation vector between $\mathbf{X}$ and $\mathbf{Y}$ before registration are randomly sampled in $[10, 20]^\circ$ and $[10, 20]$mm, respectively. The rotational error in degree is computed as

$$\theta_{\text{err}}^{\text{deg}} = \frac{\arccos[\frac{\text{trace}(\mathbf{R}_{\text{true}}\mathbf{R}_{\text{err}}^{\mathsf{T}}) - 1}{2}]}{\pi} \times 180^\circ, \tag{21}$$

while the translation error in millimeter is computed as

$$t_{\text{err}} = ||\mathbf{t}_{\text{true}} - \mathbf{t}_{\text{cal}}||_2, \tag{22}$$

where $[\mathbf{R}_{\text{cal}}, \mathbf{t}_{\text{cal}}]$ and $[\mathbf{R}_{\text{true}}, \mathbf{t}_{\text{true}}]$ are the computed and Ground-truth rigid transformation matrices. With the human pelvis model, the intra-operative points are uniformly sampled in the whole model PS while the intra-operative data is only sampled within the femur head in the case of the human femur model. $N_{\text{inliers}} = 100$ inlier points are contained in the intra-operative PS $\mathbf{X}$. In each registration case, $N_{\text{trial}} = 10000$ registration trials are conducted, whose mean registration error values in each case and with different registration methods are recorded. Six state-of-the-art registration methods are compared: ICP[50], Go-ICP [51], CPD[43], ECMPR[42], JRMPC[41], Ours (Iso). Ours (Iso) denotes the modified approach of ours by constraining $\mathbf{\Sigma}$ to be $\sigma^2\mathbf{I}_{3\times3}$, whose detailed derivations of EM procedures are omitted.

Results on the Pelvis Bone Model (Full to Full Registration) Table I includes the rotational error in degree and translation error in millimeter under both isotropic and anisotropic positional noise. The lowest error values in each test case are emphasized with bold fonts. As it can be seen from Table I, our approaches (Ours or Ours(Iso)) achieve the best registration performance (i.e., the lowest registration error values) in almost all cases. All the results have passed the statistical tests at 5% significance level. It is worth mentioning that our method owns great robustness to injected outliers (by comparing results in one same row in Table I), which is essential since outliers usually exist in the real-world intra-operative data in CAS.

Results on the Femur Bone Model (Partial to Full Registration) Table II shows the results on the human femur bone model under different cases of noise and different percentages of outliers. As it is shown in Table II, the largest mean rotational and translational error values are $\mathbf{0.6613}^\circ$ and $\mathbf{0.4608}$mm, respectively. The readers should note that all the other compared registration methods fail to register the two PSs. By comparing the results along the same columns in Table II, we can conclude that our proposed approach is stable with respect to various percentages of outliers.

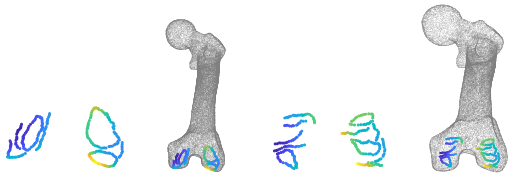

(a) Curve 1 (b) After (c) Curve 2 (d) After

Fig. 2. (a) Curve 1, (b) After Registration, (c) Curve 2, (d) After Registration. It can be seen from the figures that the intra-operative curves can be well aligned with the pre-operative model using our approach.

B. Registration Without Noise and Outliers

In all the following experiments, the human femur model is utilized and the intra-operative points only cover a partial region of the pre-operative model. The Blender software is used to select intra-operative curve from the condylar region of the human knee model (in Mesh), which is the typical region that can be touched by the surgical probe in the anterior cruciate ligament (ACL) reconstruction procedure. In all, $N_{\text{curve}} = 10$ different curves are selected from the knee model.

[1]Note that the setting of the anisotropic positional noise in the intra-operative data is realistic since that in the typical stereo camera system such as the NDI optical tracking system, the position localization error's standard deviation is usually three or five times of those in the other two orthogonal directions [46]

TABLE I
THE MEAN REGISTRATION ERROR ON THE PELVIS MODEL DATA, ROTATIONAL ERROR VALUES IN DEGREE AND THE TRANSLATION ERROR IN MM ARE PRESENTED. ISOTROPIC (DENOTED AS ISO) AND ANISOTROPIC (DENOTED AS ANISO) POSITIONAL NOISE VECTORS ARE INJECTED INTO $\mathbf{X}$, RESPECTIVELY.

	Outliers	10%	30%	50%	70%	90%	10%	30%	50%	70%	90%
		Rotational Error (in degree)					Translational Error (in mm)				
Iso	ICP[50]	0.342	1.102	1.138	1.211	0.879	0.310	0.620	0.818	1.237	1.026
	CPD[43]	2.533	2.778	2.635	3.038	3.112	2.197	2.257	2.411	2.474	2.510
	ECMPR[42]	1.863	1.843	1.942	1.549	1.481	1.483	1.375	1.392	1.172	1.153
	Go-ICP[51]	0.342	0.729	1.036	1.039	1.155	0.331	0.351	0.721	0.868	1.106
	JRMPC[41]	0.431	0.472	0.357	0.443	0.425	0.400	0.441	0.388	0.270	0.402
	Ours (Iso)	**0.326**	0.349	0.285	0.303	0.326	0.307	0.365	0.269	0.260	0.273
	Ours	0.342	**0.332**	**0.282**	**0.290**	**0.298**	**0.250**	**0.252**	**0.215**	**0.214**	**0.218**
	Outliers	10%	30%	50%	70%	90%	10%	30%	50%	70%	90%
		Rotational Error (in degree)					Translational Error (in mm)				
Aniso	ICP[50]	0.504	0.615	0.9892	1.560	1.414	**0.254**	0.561	0.520	1.002	1.123
	CPD[43]	2.059	2.256	2.191	2.522	2.715	2.035	2.188	2.276	2.219	2.342
	ECMPR[42]	1.562	1.528	1.245	1.297	1.049	1.336	1.251	1.120	1.034	0.924
	Go-ICP [51]	0.504	0.606	0.990	1.484	1.767	0.342	0.531	0.547	0.959	1.251
	JRMPC[41]	0.336	0.366	0.445	0.415	0.332	0.345	0.390	0.576	0.415	0.433
	Ours (Iso)	**0.223**	**0.128**	0.258	**0.136**	**0.126**	0.348	0.286	0.437	0.254	0.230
	Ours	0.234	0.173	**0.185**	0.156	0.158	0.290	**0.231**	**0.225**	**0.209**	**0.207**

TABLE II
THE MEAN REGISTRATION ERROR VALUES ON THE HUMAN FEMUR MODEL. THE ROTATIONAL ERROR VALUES IN DEGREE AND THE TRANSLATION ERROR IN MILIMETER ARE PRESENTED. BOTH TEST CASES WHERE ISOTROPIC AND ANISOTROPIC POSITIONAL NOISE VECTORS ARE INJECTED INTO $\mathbf{X}$ ARE PRESENTED.

	Rotational Error (in degree)		Translational Error (in mm)	
Outlier	Isotropic	Anisotropic	Isotropic	Anisotropic
10%	0.5420	0.5699	**0.4608**	0.3266
30%	0.5238	0.5965	0.3792	0.3380
50%	0.6356	0.6466	0.3378	0.3574
70%	**0.6613**	0.6412	0.3695	0.3551
90%	0.5926	0.6197	0.2865	0.3385

For each curve, hundreds of points are collected to form the intra-operative curve $\mathbf{X}$ (in average, 212 points). For example, $N_{\text{curve 1}} = 258$ and $N_{\text{curve 2}} = 171$ points exist in $\mathbf{X}$ in the first and second selected curves. The intra-operative tangent vectors $\widehat{\mathbf{X}}$ are estimated for the collected curve with the standard algorithm such as Frenet frame. In this experiment, no noise is injected into the $\mathbf{D}_x$ since the acquisition of intra-operative data is not perfect and the estimation of tangent vectors involves error. For each curve, $N_{\text{targets}} = 10$ targets are selected from the knee model to further compute the target registration error (TRE) statistics, which is defined as follows,

$$\mathbf{TRE} = \mathbf{R}_{\text{true}}\mathbf{r}_{\text{target}} + \mathbf{t}_{\text{true}} - \mathbf{R}_{\text{cal}}\mathbf{r}_{\text{target}} - \mathbf{t}_{\text{cal}} \qquad (23)$$

whose magnitude is denoted by its norm. In addition, the rotational error in degree defined in (21) and translation error in millimeter defined in (22) are also computed and recorded. Fig. 2(a) and Fig. 2(c) show the two individual intra-operative curves while Fig. 2(b) and Fig. 2(d) show the qualitative results after the registration. As can be seen from Fig. 2(c) and 2(d), the intra-operative curve is sampled from the condylar region of the human knee model (i.e., a partial region of the whole area). To emphasize, all the other compared registration methods fail in this challenging test scenario. As it is shown in Fig.2, the intra-operative curve and the pre-operative surface is well aligned. Fig. 3(a)-3(c) show the quantitative results including mean rotational(defined in (21)), translational (defined in (22)) and TRE (defined in (23)) values respectively, where N_{curve} different curves are utilized. Fig. 3(c) shows that TRE values smaller than $\mathbf{0.4}$ milimeters can be achieved with all the sampled intra-operative points and using our proposed approach. We also test the cases where only 50% intra-operative points are utilized (randomly sampled). As shown in Fig. 3(a)-3(c), the error values with 50% intra-operative points (denoted with the blue line) are smaller than the upper bound error (denoted with the green dashed line).

TABLE III
THE NUMBER OF INTRA-OPERATIVE POINTS IN DIFFERENT CURVES.

Index	1	2	3	4	5
100%	258	171	200	243	255
50%	129	86	100	122	128
Index	6	7	8	9	10
100%	233	163	168	229	196
50%	117	82	84	115	98

C. Robustness to Outliers of Our Proposed Registration Approach

In surgical navigation, the acquired intra-operative curve can easily contain outlier points due to many factors such as the surgeon's hand tremor. To further test our proposed approach's robustness to outliers, we inject outliers to the data point set $\mathbf{D}_x$. Five cases of outliers, varying from 10% outliers to 90% outliers with the interval being 20% outliers, are tested. For instance, in the case of 10% outliers, there are $N_{curve} \times 10\% = 29$ outlier points in $\mathbf{D}_x$. Fig. 4 shows both the qualitative and quantitative results under different percentages of outliers. Fig. 4(a-j) present the qualitative results, where the red points denote the intra-operative outliers. As it is shown in Fig. 4 (b,d,f,h,j), the intra-operative curves corrupted with different outlier points can be accurately aligned with the pre-operative model regardless of injected outlier points. Fig. 4 (k) includes the rotational error, the translational error and the target registration error (TRE) values defined in (21), (22) and (23) respectively. As can be seen from Fig. 4 (k), the mean rotational error values, the translation error values, and TRE values are smaller than 0.3 mm in all test cases of different outliers percentages. At the same time, the *maximum* mean rotational error values are no larger than 0.2 mm in all test

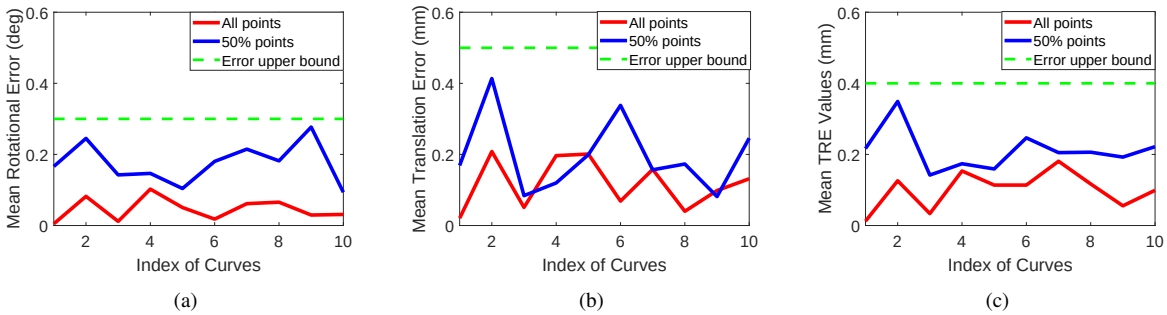

Fig. 3. (a) Mean rotational error values in degree, (b) Mean translation error values in milimeters, (c) Mean target registration error (TRE) values. In the three subfigures, the green horizon lines denote the upper error bounds.

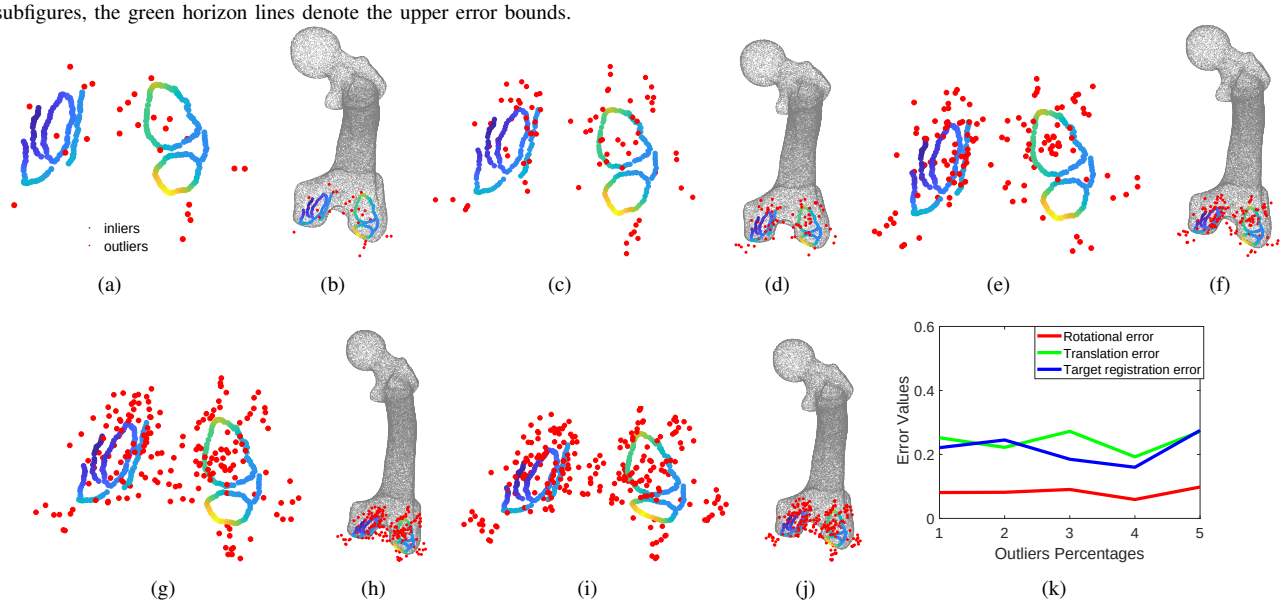

Fig. 4. Robustness to outliers is an essential characteristic to evaluate a registration approach. During surgery, the acquired intra-operative data is often contaminated with outliers that may come from sensor measurement error, surgeon's hand tremor. (a,c,e,g,i): The first intra-operative curve with different percentages of injected outliers from 10%, 30%, 50%, 70%, 90% respectively. More specifically, assume that N_{inliers} inliers points, $N_{\text{outliers}} = N_{\text{inliers}} \times 0.9$ outliers exist when there is 90% outliers. (b,d,f,h,j): The corresponding registration performances with our proposed approach used. As it can be seen from (b,d,f,h,j), the pre-operative model can be well aligned with the intra-operative data regardless of the large amount of outliers. (f) The rotational, translational and target registration error (TRE) values defined in (21), (22) and (23) under different outlier percentages. As it can be see from (f), the maximum TRE value is under 0.4 milimeters that is satisfactory.

cases. To summarize, the error values associated with test cases of different outlier percentages are quite stable with small fluctuations.

D. Robustness to Different Curve Shapes

The readers should note that in real orthopedic surgical navigation procedures, the intra-operative curves (typically acquired with an optically tracked surgical pointer in surgical navigation) could possibly have random shapes. Hence, it is also necessary to test our proposed approach's robustness to different curve shapes. Fig. 5 shows the qualitative results of registering the other eight intra-operative curves with different shapes (without outliers). As can be seen from Fig. 5, our proposed approach can well align the curve and model together in all eight test cases with different intra-operative curve shapes. Overall, $N_{curve} = 10$ different curves have been tested. Table III includes the number of inlier points in the N_{curve} test intra-operative curves. To summarize, our algorithm is very robust to the intra-operative acquired curves' shapes.

IV. Discussions

Results in Section III show that our proposed curve-to-surface registration method considering anisotropic positional uncertainties achieves significantly improved performances comapred to the existing state-of-the-art methods. With the orientational vectors extracted from two spaces to be registered, our method demonstrates great robustness to both noise and outliers. Results in Table I verify the advantage of considering the anisotropic positional uncertainty since our proposed approach achieves the best registration performances in 14 out of all 20 test cases. More importantly, all the methods that only use the positional information have failed to align the partial intra-operative curve with the whole pre-operative model while our approach can still own high accuracy as suggested by results in Table II. Our method has also been

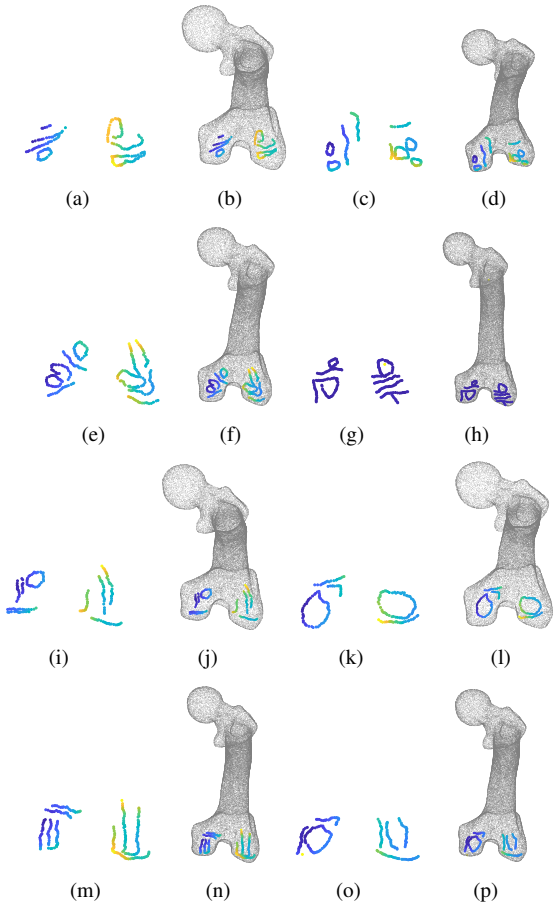

Fig. 5. The remaing eight different intra-operative curves (a,c,e,g,i,k,m,o) and their corresponding registration performances (b,d,f,h,j,l,n,p) with our proposed registration approach.

validated to own great robustness to noise and outliers, and to different curves' shapes. Limitations: The first limitation with our proposed method is that only a limited range of rotation angles can be accommodated. In other words, our proposed registration approach is a locally optimal registration method. This limitation is because that our proposed algorithm is developed based on the Gaussian mixture models (GMMs) and Coherent Point Drift (CPD) theories. One usual strategy can be used that is, several anatomical landmarks or fiducials can be used and their physical locations in the pre-operative and intra-operative spaces are utilized to complete the initial coarse registration task. The second limitation is that we only consider the anisotropy in the positional information. The error associated with the normal vectors is assumed to be isotropic in the proposed approach. This limitation comes from the use of von-Mises fisher distribution where the isotropic orientation error is assumed. The third limitation is the computational speed is slow with respect to those using only positional information, despite that we have derived and utilized the matrix forms of several parameters such as the updated positional covariance matrix in the maximization step. This limitation also comes from the use of Gaussian mixture models (GMMs). It should also be noted that all the experiments have been performed on simulated or synthetic data. While it gives convenience to benchmark our proposed registration approach against others, the improvements on the real-world data may be different to some extent.

Future Work: The first useful direction is to develop a global registration approach that eliminates the needs for an additional coarse registration step. One potential solution is to select a subset of the position+tangent or position+normal pairs, and then establish their pair correspondences. After that, the coarse rigid transformation matrix can be computed using variant algorithms in the Maxmization Transformation step in this paper. To overcome the second limitation, the Kent distribution can be used to model the error associated with the normal/tangent vectors. To overcome the third limitation, the Matlab codes can be substituted with C++ version to further accelerate the algorithm. It will be interesting to adopt the deep learning technique such as convolution neural networks (CNNs) to estimate the normal/tangent vectors from the raw point sets, which has been demonstrated to be more accurate and robust compared to conventional methods [53]. The estimated normal and tangent vectors can be further readily incorporated into our registration framework.

V. Conclusions

In this article, we present a novel registration approach to compute the rigid transformation matrix between the pre-operative space *and* the intra-operative space in computer-assisted orthopedic surgery (CAOS). In addition to the positional information, the normal vectors extracted from the pre-operative surface and the tangent vectors extracted from the intra-operative curve are utilized in proposed registration algorithm. The position localization error is assumed to be anisotropic, which is a generalized assumption of the isotropic positional error. Our proposed approach has been demonstrated to be accurate and robust to noise, outliers (e.g., 90% outliers) with extensive simulated experiments.

VI. Appendix

A. Von-Mises Fisher distribution

In this section, we briefly introduce the basics of von-Mises-Fisher (vMF) distribution that is used to model the orientation-al error. The probability density function of the vMF distribution for the random d-dimensional unit vector $\widehat{\mathbf{x}}$ (i.e. $\widehat{\mathbf{x}} \in \mathbb{R}^d$ and $||\widehat{\mathbf{x}}|| = 1$, or equivalently $\widehat{\mathbf{x}} \in \mathbb{S}^{d-1}$) is given by

$$p(\widehat{\mathbf{x}}|\widehat{\boldsymbol{\mu}}, \kappa) = c_d(\kappa) e^{\kappa \widehat{\boldsymbol{\mu}}^{\mathsf{T}} \widehat{\mathbf{x}}} \tag{24}$$

where $||\widehat{\boldsymbol{\mu}}|| = 1$, $\kappa \geq 0$ and $d \geq 2$. The normalizing constant $c_d(\kappa)$ is the following:

$$c_d(\kappa) = \frac{\kappa^{d/2-1}}{(2\pi)^{d/2} I_{d/2-1}(\kappa)} \tag{25}$$

where $I_r(\bullet)$ denotes the modified Bessel function of the first kind and order r. The above density function $p(\widehat{\mathbf{x}}|\widehat{\boldsymbol{\mu}}, \kappa)$ is parameterized by the mean direction $\widehat{\boldsymbol{\mu}}$ and the concentration parameter κ. We remark that larger values of κ indicate

stronger concentration about the mean direction. More specifically, in our case (where $d = 3$), the normalizing constant $c_d(\kappa)$ is the following:

$$c_d(\kappa) = \frac{\kappa}{2\pi(e^{\kappa} - e^{-\kappa})} \tag{26}$$

The vMF distribution is one of the simplest parametric distributions for the orientation-al data.

B. The Derivation of $C_{N,mn}$ in (9)

Recall that the original formulation of $C_{N,mn}$ in (7) is as the following

$$\begin{aligned} C_{N,mn} &= -p_{mn}^{q}\kappa\Big|\Big|(d\mathbf{R}\mathbf{R}^{q-1}\widehat{\mathbf{y}}_m) \times \widehat{\mathbf{x}}_n\Big|\Big| \\ &= -p_{mn}^{q}\kappa sin(\alpha) = -p_{mn}^{q}\kappa\sqrt{1-\cos^2(\alpha)}, \\ &= -p_{mn}^{q}\kappa\sqrt{1-(\widehat{\mathbf{y}}_m^{\mathsf{T}}\mathbf{R}^{\mathsf{T}}d\mathbf{R}^{\mathsf{T}}\mathbf{x}_n)^2} \end{aligned} \tag{27}$$

where we denote $\alpha \in \mathbb{R}$ as the angle between $d\mathbf{R}\mathbf{R}^{q-1}\widehat{\mathbf{y}}_m$ and $\widehat{\mathbf{x}}_n$.

C. The Derivation of $\frac{\partial \mathbf{C}_{N,mn}}{\partial d\mathbf{R}}$ in (11)

For clarity, we present again the full expression of $\mathbf{C}_{N,mn}$ as follows,

$$\mathbf{C}_{N,mn} = -p_{mn}\kappa\sqrt{1-(\widehat{\mathbf{y}}_m\mathbf{R}^{\mathsf{T}}d\mathbf{R}^{\mathsf{T}}\widehat{\mathbf{X}}_n)^2} \tag{28}$$

Let the scalar a be defined as

$$a = 1-(\widehat{\mathbf{y}}_m\mathbf{R}^{\mathsf{T}}d\mathbf{R}^{\mathsf{T}}\widehat{\mathbf{X}}_n)^2 = 1-\widehat{\mathbf{x}}_n^{\mathsf{T}}d\mathbf{R}\mathbf{R}\widehat{\mathbf{y}}_m^{\mathsf{T}}\widehat{\mathbf{y}}_m\mathbf{R}^{\mathsf{T}}d\mathbf{R}^{\mathsf{T}}\widehat{\mathbf{x}}_n \tag{29}$$

With the *Chain rule* of derivatives, we can easily get the following expression of $\frac{\partial \mathbf{C}_{N,mn}}{\partial d\mathbf{R}}$,

$$\frac{\partial \mathbf{C}_{N,mn}}{\partial d\mathbf{R}} = \frac{\partial \mathbf{C}_{N,mn}}{\partial a}\frac{\partial a}{\partial d\mathbf{R}} \tag{30}$$

where

$$\frac{\partial \mathbf{C}_{N,mn}}{\partial a} = -p_{mn}\kappa\frac{1}{2}a^{-\frac{1}{2}}. \tag{31}$$

With the formula $\frac{\partial \mathbf{b}^{\mathsf{T}}\mathbf{X}^{\mathsf{T}}\mathbf{D}\mathbf{X}\mathbf{c}}{\partial \mathbf{b}} = \mathbf{D}^{\mathsf{T}}\mathbf{X}\mathbf{b}\mathbf{c}^{\mathsf{T}} + \mathbf{D}\mathbf{X}\mathbf{c}\mathbf{b}^{\mathsf{T}}$ where $\mathbf{D}$ and $\mathbf{X}$ are random matrices, the derivative of a in (29) with respect to $d\mathbf{R}$ $\frac{\partial a}{\partial d\mathbf{R}}$ is

$$\frac{\partial a}{\partial d\mathbf{R}} = -\widehat{\mathbf{y}}_m^{\mathsf{T}}\widehat{\mathbf{y}}_m\mathbf{R}^{\mathsf{T}}d\mathbf{R}\widehat{\mathbf{x}}_n\widehat{\mathbf{x}}_n^{\mathsf{T}}. \tag{32}$$

Now we can get the full expression of $\frac{\partial \mathbf{C}_{N,mn}}{\partial d\mathbf{R}}$ in (10) with (30), (31), (29) and (32), which is presented as follows,

$$p_{mn}\kappa\frac{1}{2}(1-(\widehat{\mathbf{y}}_m\mathbf{R}^{\mathsf{T}}d\mathbf{R}^{\mathsf{T}}\widehat{\mathbf{X}}_n)^2)^{-\frac{1}{2}}\widehat{\mathbf{y}}_m^{\mathsf{T}}\widehat{\mathbf{y}}_m\mathbf{R}^{\mathsf{T}}d\mathbf{R}\widehat{\mathbf{x}}_n\widehat{\mathbf{x}}_n^{\mathsf{T}}. \tag{33}$$

D. The Expressions of $\frac{\partial d\mathbf{R}}{\partial d\theta_1}$, $\frac{\partial d\mathbf{R}}{\partial d\theta_2}$, and $\frac{\partial d\mathbf{R}}{\partial d\theta_3}$ in (11)

$$\begin{cases} \dfrac{\partial \mathsf{sk}(d\boldsymbol{\theta})}{\partial d\theta_1} = \underbrace{\begin{bmatrix} 0 & 0 & 0 \\ 0 & 0 & -1 \\ 0 & 1 & 0 \end{bmatrix}}_{\mathbf{A}^1} & \dfrac{\partial \mathsf{sk}(d\boldsymbol{\theta})}{\partial d\theta_2} = \underbrace{\begin{bmatrix} 0 & 0 & 1 \\ 0 & 0 & 0 \\ -1 & 0 & 0 \end{bmatrix}}_{\mathbf{A}^2} \\ \dfrac{\partial \mathsf{sk}(d\boldsymbol{\theta})}{\partial d\theta_3} = \underbrace{\begin{bmatrix} 0 & -1 & 0 \\ 1 & 0 & 0 \\ 0 & 0 & 0 \end{bmatrix}}_{\mathbf{A}^3} \end{cases}. \tag{34}$$

E. The Expression of $\frac{\partial \mathbf{C}_{P,mn}}{\partial d\mathbf{t}}$ in (12)

$$\frac{\partial \mathbf{C}_{P,mn}}{\partial d\mathbf{t}} = (\boldsymbol{\Sigma}^{q-1})^{-1}\Big(-\mathbf{x}_n + d\mathbf{t} + d\mathbf{R}\big(\mathbf{R}^{q-1}\mathbf{y}_m + \mathbf{t}^{q-1}\big)\Big). \tag{35}$$

VII. Acknowledgement

The work of Prof. Max Q.-H. Meng was supported in part by the Hong Kong Research Grants Council (RGC) General Research Fund (GRF) under Grant 14210117, the Hong Kong Research Grants Council (RGC) General Research Fund (GRF) under Grant 14211420, the RGC NSFC/RGC Joint Research Scheme under Grant N_CUHK448/17, the Shenzhen Science and Technology Innovation projects under Grant JCYJ20170413161616163, National Key RD program of China with Grant No. 2019YFB1312400, and in part by the Hong Kong RGC Theme-based Research Scheme (TRS) grant T42-409/18-R. The work of Prof. Hongliang Ren was supported by the Shun Hing Institute of Advanced Engineering (SHIAE project BME-p1-21) at the Chinese University of Hong Kong (CUHK). The authors would like to thank deeply the anonymous reviewers for their precious comments that have significantly improved the paper's quality.

References

[1] C. Raposo, C. Sousa, L. Ribeiro, R. Melo, J. P. Barreto, J. Oliveira, P. Marques, and F. Fonseca, "Video-based computer aided arthroscopy for patient specific reconstruction of the anterior cruciate ligament," in *International Conference on Medical Image Computing and Computer-Assisted Intervention*. Springer, 2018, pp. 125–133.

[2] C. Raposo, J. P. Barreto, C. Sousa, L. Ribeiro, R. Melo, J. P. Oliveira, P. Marques, F. Fonseca, and D. Barrett, "Video-based computer navigation in knee arthroscopy for patient-specific acl reconstruction," *International journal of computer assisted radiology and surgery*, vol. 14, no. 9, pp. 1529–1539, 2019.

[3] G. Samitier, A. I. Marcano, E. Alentorn-Geli, R. Cugat, K. W. Farmer, and M. W. Moser, "Failure of anterior cruciate ligament reconstruction," *Archives of bone and joint surgery*, vol. 3, no. 4, p. 220, 2015.

[4] R. H. Taylor, L. Joskowicz, B. Williamson, A. Guéziec, A. Kalvin, P. Kazanzides, R. Van Vorhis, J. Yao, R. Kumar, A. Bzostek *et al.*, "Computer-integrated revision total hip replacement surgery: concept and preliminary results," *Medical image analysis*, vol. 3, no. 3, pp. 301–319, 1999.

[5] W. Du, T. Sun, Y. Ding, C. Jiang, W. Qu, and S. Zhang, "Robot-assisted treatment of unstable pelvic fractures with a percutaneous iliac lumbar double rod fixation combined with a percutaneous pelvic anterior ring infix fixation," *International Orthopaedics*, vol. 44, no. 6, p. 1223, 2020.

[6] R. H. Taylor, P. Kazanzides, G. S. Fischer, and N. Simaan, "Medical robotics and computer-integrated interventional medicine," in *Biomedical Information Technology*. Elsevier, 2020, pp. 617–672.

[7] J.-X. Zhao, C. Li, H. Ren, M. Hao, L.-C. Zhang, and P.-F. Tang, "Evolution and current applications of robot-assisted fracture reduction: a comprehensive review," *Annals of biomedical engineering*, vol. 48, no. 1, pp. 203–224, 2020.

[8] T. Vercauteren, M. Unberath, N. Padoy, and N. Navab, "Cai4cai: The rise of contextual artificial intelligence in computer-assisted interventions," *Proceedings of the IEEE*, vol. 108, no. 1, pp. 198–214, 2019.

[9] H. Ren and P. Kazanzides, "Investigation of attitude tracking using an integrated inertial and magnetic navigation system for hand-held surgical instruments," *IEEE/ASME Transactions on Mechatronics*, vol. 17, no. 2, pp. 210–217, 2010.

[10] H. Ren, D. Rank, M. Merdes, J. Stallkamp, and P. Kazanzides, "Multisensor data fusion in an integrated tracking system for endoscopic surgery," *IEEE Transactions on Information Technology in Biomedicine*, vol. 16, no. 1, pp. 106–111, 2011.

[11] H. Ren, C. M. Lim, J. Wang, W. Liu, S. Song, Z. Li, G. Herbert, Z. T. H. Tse, and Z. Tan, "Computer-assisted transoral surgery with flexible robotics and navigation technologies: A review of recent progress and research challenges," *Critical Reviews™ in Biomedical Engineering*, vol. 41, no. 4-5, 2013.

[12] J. Wang, M. Q.-H. Meng, and H. Ren, "Towards occlusion-free surgical instrument tracking: A modular monocular approach and an agile calibration method," *IEEE Transactions on Automation Science and Engineering*, vol. 12, no. 2, pp. 588–595, 2015.

[13] J. Wang, S. Song, H. Ren, C. M. Lim, and M. Q.-H. Meng, "Surgical instrument tracking by multiple monocular modules and a sensor fusion approach," *IEEE Transactions on Automation Science and Engineering*, vol. 16, no. 2, pp. 629–639, 2018.

[14] J. Luo, S. Frisken, I. Machado, M. Zhang, S. Pieper, P. Golland, M. Toews, P. Unadkat, A. Sedghi, H. Zhou *et al.*, "Using the variogram for vector outlier screening: application to feature-based image registration," *Int. J. Comput. Assist. Radiol. Surg.*, vol. 13, no. 12, pp. 1871–1880, 2018.

[15] J. Luo, A. Sedghi, K. Popuri, D. Cobzas, M. Zhang, F. Preiswerk, M. Toews, A. Golby, M. Sugiyama, W. M. Wells *et al.*, "On the applicability of registration uncertainty," in *International Conference on Medical Image Computing and Computer-Assisted Intervention*. Springer, 2019, pp. 410–419.

[16] M. R. Robu, J. Ramalhinho, S. Thompson, K. Gurusamy, B. Davidson, D. Hawkes, D. Stoyanov, and M. J. Clarkson, "Global rigid registration of ct to video in laparoscopic liver surgery," *Int. J. Comput. Assist. Radiol. Surg.*, vol. 13, no. 6, pp. 947–956, 2018.

[17] J. Ma, Y. Ma, and C. Li, "Infrared and visible image fusion methods and applications: A survey," *Information Fusion*, vol. 45, pp. 153–178, 2019.

[18] J. Wu, "Rigid 3d registration: A simple method free of svd and eigendecomposition," *IEEE Transactions on Instrumentation and Measurement*, 2020.

[19] J. Wu, M. Liu, Z. Zhou, and R. Li, "Fast symbolic 3-d registration solution," *IEEE Transactions on Automation Science and Engineering*, vol. 17, no. 2, pp. 761–770, 2019.

[20] J. Ma, J. Zhao, J. Jiang, H. Zhou, and X. Guo, "Locality preserving matching," *International Journal of Computer Vision*, vol. 127, no. 5, pp. 512–531, 2019.

[21] J. Ma, X. Jiang, J. Jiang, J. Zhao, and X. Guo, "Lmr: Learning a two-class classifier for mismatch removal," *IEEE Transactions on Image Processing*, vol. 28, no. 8, pp. 4045–4059, 2019.

[22] J. Ma, X. Jiang, J. Jiang, and Y. Gao, "Feature-guided gaussian mixture model for image matching," *Pattern Recognition*, vol. 92, pp. 231–245, 2019.

[23] J. Zhou, X. Ma, L. Liang, Y. Yang, S. Xu, Y. Liu, and S.-H. Ong, "Robust variational bayesian point set registration," in *Proceedings of the IEEE International Conference on Computer Vision*, 2019, pp. 9905–9914.

[24] J. Serafin and G. Grisetti, "Nicp: Dense normal based point cloud registration," in *2015 IEEE/RSJ International Conference on Intelligent Robots and Systems (IROS)*. IEEE, 2015, pp. 742–749.

[25] S. Billings and R. Taylor, "Iterative most likely oriented point registration," in *International Conference on Medical Image Computing and Computer-Assisted Intervention*. Springer, 2014, pp. 178–185.

[26] ——, "Generalized iterative most likely oriented-point (g-imlop) registration," *International journal of computer assisted radiology and surgery*, vol. 10, no. 8, pp. 1213–1226, 2015.

[27] S. Bayer, N. Ravikumar, M. Strumia, X. Tong, Y. Gao, M. Ostermeier, R. Fahrig, and A. Maier, "Intraoperative brain shift compensation using a hybrid mixture model," in *International Conference on Medical Image Computing and Computer-Assisted Intervention*. Springer, 2018, pp. 116–124.

[28] S. Bayer, Z. Zhai, M. Strumia, X. Tong, Y. Gao, M. Staring, B. Stoel, R. Fahrig, A. Nabavi, A. Maier *et al.*, "Registration of vascular structures using a hybrid mixture model," *International journal of computer assisted radiology and surgery*, vol. 14, no. 9, pp. 1507–1516, 2019.

[29] Z. Min, J. Wang, and M. Q.-H. Meng, "Robust generalized point cloud registration using hybrid mixture model," in *2018 IEEE International Conference on Robotics and Automation*. IEEE, 2018, pp. 4812–4818.

[30] N. Ravikumar, "A probabilistic framework for statistical shape models and atlas construction: Application to neuroimaging," Ph.D. dissertation, University of Sheffield, 2017.

[31] N. Ravikumar, A. Gooya, L. Beltrachini, A. F. Frangi, and Z. A. Taylor, "Generalised coherent point drift for group-wise multi-dimensional analysis of diffusion brain mri data," *Med. Image. Anal.*, 2019.

[32] N. Ravikumar, A. Gooya, A. F. Frangi, and Z. A. Taylor, "Generalised coherent point drift for group-wise registration of multi-dimensional point sets," in *International Conference on Medical Image Computing and Computer-Assisted Intervention*. Springer, 2017, pp. 309–316.

[33] A. Sinha, X. Liu, A. Reiter, M. Ishii, G. D. Hager, and R. H. Taylor, "Endoscopic navigation in the absence of ct imaging," in *International Conference on Medical Image Computing and Computer-Assisted Intervention*. Springer, 2018, pp. 64–71.

[34] Z. Min, L. Liu, and M. Q.-H. Meng, "Generalized non-rigid point set registration with hybrid mixture models considering anisotropic positional uncertainties," in *International Conference on Medical Image Computing and Computer-Assisted Intervention*. Springer, 2019, pp. 547–555.

[35] J. Luo, M. Toews, I. Machado, S. Frisken, M. Zhang, F. Preiswerk, A. Sedghi, H. Ding, S. Pieper, P. Golland *et al.*, "A feature-driven active framework for ultrasound-based brain shift compensation," in *International Conference on Medical Image Computing and Computer-Assisted Intervention*. Springer, 2018, pp. 30–38.

[36] Y. Aoki, H. Goforth, R. A. Srivatsan, and S. Lucey, "Pointnetlk: Robust & efficient point cloud registration using pointnet," in *Proceedings of the IEEE Conference on Computer Vision and Pattern Recognition*, 2019, pp. 7163–7172.

[37] Y. Wang and J. M. Solomon, "Deep closest point: Learning representations for point cloud registration," in *Proceedings of the IEEE International Conference on Computer Vision*, 2019, pp. 3523–3532.

[38] ——, "Prnet: Self-supervised learning for partial-to-partial registration," in *Advances in Neural Information Processing Systems*, 2019, pp. 8812–8824.

[39] J. Ma, X. Jiang, A. Fan, J. Jiang, and J. Yan, "Image matching from handcrafted to deep features: A survey," *International Journal of Computer Vision*, pp. 1–57, 2020.

[40] Q.-Y. Zhou, J. Park, and V. Koltun, "Fast global registration," in *European Conference on Computer Vision*. Springer, 2016, pp. 766–782.

[41] G. D. Evangelidis and R. Horaud, "Joint alignment of multiple point sets with batch and incremental expectation-maximization," *IEEE Transactions on Pattern Analysis and Machine Intelligence*, 2017.

[42] R. Horaud, F. Forbes, M. Yguel, G. Dewaele, and J. Zhang, "Rigid and articulated point registration with expectation conditional maximization," *IEEE Transactions on Pattern Analysis and Machine Intelligence*, vol. 33, no. 3, pp. 587–602, 2011.

[43] A. Myronenko and X. Song, "Point set registration: Coherent point drift," *IEEE transactions on pattern analysis and machine intelligence*, vol. 32, no. 12, pp. 2262–2275, 2010.

[44] R. B. Rusu, N. Blodow, and M. Beetz, "Fast point feature histograms (fpfh) for 3d registration," in *2009 IEEE international conference on robotics and automation*. IEEE, 2009, pp. 3212–3217.

[45] Z. Min, J. Wang, S. Song, and M. Q.-H. Meng, "Robust generalized point cloud registration with expectation maximization considering anisotropic positional uncertainties," in *2018 IEEE/RSJ International Conference on Intelligent Robots and Systems (IROS)*. IEEE, 2018, pp. 1290–1297.

[46] L. Maier-Hein, P. Mountney, A. Bartoli, H. Elhawary, D. Elson, A. Groch, A. Kolb, M. Rodrigues, J. Sorger, S. Speidel *et al.*, "Optical techniques for 3d surface reconstruction in computer-assisted laparoscopic surgery," *Medical image analysis*, vol. 17, no. 8, pp. 974–996, 2013.

[47] S. D. Billings, E. M. Boctor, and R. H. Taylor, "Iterative most-likely point registration (imlp): A robust algorithm for computing optimal shape alignment," *PloS one*, vol. 10, no. 3, p. e0117688, 2015.

[48] Z. Min, J. Wang, and M. Q.-H. Meng, "Robust generalized point cloud registration with orientational data based on expectation maximization," *IEEE Transactions on Automation Science and Engineering*, vol. 17, no. 1, pp. 207–221, 2020.

[49] ——, "Joint rigid registration of multiple generalized point sets with hybrid mixture models," *IEEE Transactions on Automation Science and Engineering*, vol. 17, no. 1, pp. 334–347, 2020.

[50] Z. Zhang, "Iterative point matching for registration of free-form curves and surfaces," *International journal of computer vision*, vol. 13, no. 2, pp. 119–152, 1994.

[51] J. Yang, H. Li, D. Campbell, and Y. Jia, "Go-icp: A globally optimal solution to 3d icp point-set registration," *IEEE Transactions on Pattern Analysis & Machine Intelligence*, no. 11, pp. 2241–2254, 2016.

[52] S. D. Billings, E. M. Boctor, and R. H. Taylor, "Iterative most-likely point registration (imlp): a robust algorithm for computing optimal shape alignment," *PloS one*, vol. 10, no. 3, 2015.

[53] Y. Ben-Shabat, M. Lindenbaum, and A. Fischer, "Nesti-net: Normal estimation for unstructured 3d point clouds using convolutional neural

networks," in *2019 IEEE/CVF Conference on Computer Vision and Pattern Recognition (CVPR)*, 2019, pp. 10 104–10 112.

Zhe Min (Member, IEEE) received the Ph.D. degree in Electronic Engineering from the Chinese University of Hong Kong, Hong Kong, China, in 2019. Afterwards, he was a Postdoc Fellow at the Department of Electronic Engineering in the Chinese University of Hong Kong (CUHK), Hong Kong. He is now a Research Fellow with the Department of Medical Physics and Bioengineering, University College London, London, United Kingdom.

He has served as one program committee in CISRAM 2017. He was a recipient of the IROS 2017 Travel Award and ICRA 2019 Travel Award funded by the IEEE Robotics and Automation Society, and the International Society for Computer Aided Surgery (ISCAS) Travel Award to attend Computer Assisted Radiology and Surgery (CARS) 2018 congress. He was also a receipt of the Research Fellowship Scheme 2020-2021 awarded by Faculty of Engineering, CUHK. He is a reviewer of MICCAI 2018-2021, ISBI 2021, IROS 2020 and a regular reviewer in several international journals such as Information Fusion, IEEE Transactions on Cybernetics (T-Cyber), IEEE Transactions on Automation Science and Engineering (T-ASE), IEEE Transactions on Image Processing (TIP), IEEE/CAA Journal of Automatica Sinica (JAS), Annuals of Biomedical Engineering (ABME), Robotics and Automation Letters (RAL), IEEE Sensors Journal, and International Journal of Computer Assisted Radiology and Surgery (IJCARS). His current research interests include surgical navigation, medical robotics and surface registration algorithms.

Delong Zhu received the Ph.D. degree in electronic engineering from the Chinese University of Hong Kong, Hong Kong, China, in 2020. He is currently a research associate in Department of Electronic Engineering at The Chinese University of Hong Kong, Shatin, N.T., Hong Kong. His research interest includes deep learning, robotic perception, and motion planning. He has published several papers in ICRA, IROS and RAL.

Jianbang Liu received the B.E. degree in microelectronics from Sun Yat-sen University, B.E. degree in electronic engineering from the Hong Kong Polytechnic University in 2015, and M.Sc. degree from the University of Hong Kong in 2016. Currently, he is working toward the Ph.D. degree at the Chinese University of Hong Kong. His research interests include sensor fusion, 3D pose estimation and robotic vision.

Hongliang Ren (M'06–SM'17) received the Ph.D. degree in electronic engineering with a specialization in biomedical engineering from The Chinese University of Hong Kong, Hong Kong, in 2008.

He was a Research Fellow with the Laboratory for Computational Sensing and Robotics and the Engineering Center for Computer-Integrated Surgical Systems and Technology, Department of Biomedical Engineering and the Department of Computer Science, Johns Hopkins University, Baltimore, MD, USA, from 2008 to 2010. In 2010, he joined the Pediatric Cardiac Biorobotics Laboratory, Department of Cardiovascular Surgery, Children's Hospital Boston, Boston, MA, USA, and the Harvard Medical School, Boston, for investigating the beating heart robotic surgery system. In 2012, he was with the Collaborative Computer Integrated Surgery Project, Surgical Innovation Institute, Children's National Medical Center, Washington, DC, USA. He is an Associate Professor in the Department of Electronic Engineering in the Chinese University of Hong Kong. He was an Assistant Professor and leading a research group on medical mechatronics with the Biomedical Engineering Department, National University of Singapore, Singapor. His research interests include intelligent systems, mechatronics, signal processing, computerintegrated surgery, and dynamic positioning in medicine.

Max Q.-H. Meng (M'92-F'07) received the Ph.D. degree in electrical and computer engineering from the University of Victoria, Victoria, BC, Canada, in 1992.

He is now a Professor and Chairman of the Department of Electronic and Electrical Engineering of the Southern University of Science and Technology in Shenzhen, China, on leave from the Department of Electronic Engineering, The Chinese University of Hong Kong, Hong Kong, and also with the Shenzhen Research Institute of the Chinese University of Hong Kong in Shenzhen, China. He has been a Professor of electronic engineering with the Chinese University of Hong Kong (CUHK), Hong Kong, since 2002, after being the Director of the ART (Advanced Robotics and Teleoperation) Lab and Professor for ten years with the Department of Electrical and Computer Engineering, University of Alberta, Edmonton, AB, Canada. He has authored over 500 journal and conference papers.

His current research interests include robotics, perception and sensing, human robot interaction, active medical devices, biosensors and sensor networks, and adaptive and intelligent systems. Prof. Meng is an Elected Member of the Administrative Committee of the IEEE Robotics and Automation Society and has served on many editorial boards. He is a recipient of the IEEE Millennium Medal, a Fellow of IEEE, a Fellow of Hong Kong Institution of Engineers, and a Fellow of the Canadian Academy of Engineering.